ChemComm

FEATURE ARTICLE

View Article Online
View Journal

Cite this: DOI: 10.1039/d3cc04048h

New opportunities for cyclodextrins in supramolecular assembly: metal organic frameworks, crystalline self-assembly, and catalyzed assembly

Ting Gu, Jianbin Huang* and Yun Yan *

Cyclodextrins (CDs) are widely used macrocycles in supramolecular assembly due to their easy availability, versatile functionality and excellent biocompatibility. Although they are well-known for forming host–guest complexes with a wide range of guests and this host–guest chemistry has long been utilized in industry and academia, new opportunities have arisen in recent years, particularly in supramolecular assembly. In the present review, we will first provide a basic introduction to CDs and then summarize their emerging roles in the fields of supramolecular chemistry and materials. This includes their involvement in hybrid frameworks with inorganic components such as metal ions and polyoxometalates, crystalline self-assembly with amphiphilic molecules, and their new possibility of "catassembly" and induced chiral supramolecular structures that have previously been overlooked. Finally, we will comment on the future perspectives of CDs to inspire more ideas and efforts, with the aim of promoting diverse applications of CDs in supramolecular materials.

Received 21st August 2023,
Accepted 13th November 2023

DOI: 10.1039/d3cc04048h

rsc.li/chemcomm

1 Introduction

Cyclodextrins (CDs) are cyclic oligosaccharides produced through the enzymatic degradation of starch. They are composed of several D-pyranose units linked by 1,4-glycosidic bonds, forming a cyclic structure that has a toroidal shape with a primary and a secondary face. CDs of practical value are α-CD, β-CD and γ-CD, which consist of six, seven and eight D-pyranose units, respectively (Fig. 1). As early as 1984, they could be produced in a highly pure form at a low cost, which greatly contributed to their practical application. The molecular height of all CDs is approximately 0.78 nm and the inner diameter of their cavities increases gradually from α-CD to γ-CD, namely, 0.57, 0.78 and 0.95 nm, respectively. Besides the three "native" CDs, numerous CD derivatives have been designed and synthesized through chemical modification of the hydroxyl groups at C-2, C-3, and C-6. These CD derivatives exhibit modified or enhanced properties that can better meet specific demands. For example, hydroxypropyl-β-CD (HP-β-CD), which is produced by partially substituting hydroxypropyl groups, has significantly improved water solubility compared to β-CD. This improvement can be attributed to the damage of the intramolecular hydrogen bond belt in pristine β-CD.[1] At present, CDs are extensively employed in all practical sectors of industry, including pharmacy,[2–4] food,[5–7] chromatography,[8,9] agriculture,[10] cosmetics and toiletries,[11] and environment.[12–14]

The most prominent feature of a CD's structure is its dimensionally stable cavity. The inner wall of the cavity is covered with glycosidic oxygen and C–H units. As a result, the

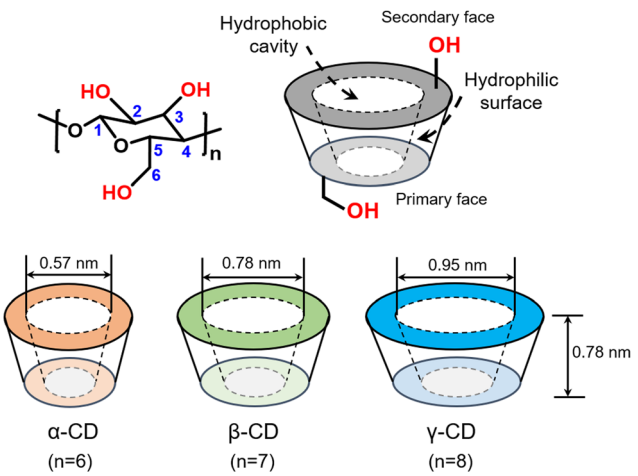

Fig. 1 Structures and approximate geometric dimensions of α-CD, β-CD and γ-CD.

Beijing National Laboratory for Molecular Sciences (BNLMS), State Key Laboratory for Structural Chemistry of Unstable and Stable Species, College of Chemistry and Molecular Engineering, Peking University, Beijing, 100871, P. R. China.
E-mail: yunyan@pku.edu.cn

cavity is hydrophobic and less polar than water. In contrast, the outer surface of CDs contains numerous hydroxyl groups, which makes it soluble in water. As a result, hydrophobic species, such as molecules and nanoparticles, can be encapsulated within the cavity of CDs, forming inclusion complexes. Notably, complexation is the result of synergistic cooperation among multiple noncovalent interactions, such as hydrophobic interactions, hydrogen bonding, van der Waals forces, and so on. These noncovalent host–guest interactions are highly reversible and dynamic in solution. The complexation of guests into the cavity of CDs can significantly modify or enhance their physical, chemical or biological characteristics, laying the foundation for their practical application in various fields.

Dating back to the 1970s, exploration of CD applications was initiated in the pharmaceutical field. At that time, CDs emerged as an effective approach to enhance the water solubility of hydrophobic drugs while causing little irritation, thereby greatly improving drug efficiency. The first product, prostaglandin E2/β-CD Prostarmon E™ sublingual tablet, was marketed by Japan (Ono Pharmaceutical Co.) in 1976.[2,15] To date, there have been over 40 different drugs marketed worldwide in the form of CD complexes. Besides, the application fields of CDs have quickly expanded to include traditional industries such as food, cosmetics, toiletries and agriculture. For example, CDs have been widely used to improve the stability of food additives[16] or to mask the unpleasant taste of food ingredients.[17] So far, people's interest in CDs has shifted from their practical usage in industry sectors to more state-of-the-art academic areas, such as computational chemistry and supramolecular assembly.

In the field of supramolecular assembly, CDs have always played an active role in the synthesis of novel supramolecular architectures. In the 1990s, Stoddart reported the first case of an α-CD-based catenane.[18] Akira Harada constructed a variety of polyrotaxanes with exquisite structures using CDs and poly(ethylene glycol) (PEG).[19–21] The last two decades have witnessed many new possibilities of CDs in the field of supramolecular materials. For instance, CDs have been found to be capable of assembling with inorganic components such as metal ions[22] and polyoxometalates[23–26] to form extended three-dimensional frameworks. Crystalline self-assemblies based on CD complexes can be driven by hydrogen bonds between CDs, exhibiting high rigidity that mimics protein assembly in nature.[27–30] In some cases, CDs can play the role of a "catalyst" in facilitating the formation of specific assembled structures.[31–33] In addition, although the chiral nature of CDs has long been recognized and they are widely used in chiral separations,[34–36] an increasing number of studies have shown that their full potential has not been explored, particularly in the development of supramolecular chiral materials.[37–42] These new findings have greatly enhanced our understanding of CDs. For this reason, we aim to provide a conceptual summary in this short review, with the goal of attracting more attention to CDs and encouraging future exploration.

2 CD-based hybrid frameworks

CDs are rich in hydroxyl groups, which enables them to interact with specific inorganic components such as metal ions or polyoxometalates, facilitating the construction of hybrid framework structures. In particular, CDs can serve as ligands and directly coordinate with metal ions to form metal–organic frameworks (MOFs). The role of metal ions can also be replaced by polyoxometalates to form supramolecular hybrid frameworks. In the following, we will discuss two categories of CD-based hybrid frameworks.

2.1 MOFs based on CDs and metal ions

2.1.1 Formation principle. Metal–organic frameworks (MOFs) are a type of porous crystalline material formed by organic ligands as linkers and metal ions or clusters as nodes through coordination interactions.[43–45] CDs were not associated with MOFs until Stoddart and co-workers reported the first case of CD-based MOFs using the vapor diffusion method in 2010[22] (Fig. 2a). Since then, numerous CD-based MOFs with unique topologies have been synthesized using α-CD and β-CD. Additionally, the range of metal ions used has expanded from alkali to alkaline and even transition metal ions.[46–49] Besides vapor diffusion,[22,50] a variety of synthetic methods have been proposed, including microwave-assisted,[51] hydro/solvothermal[52,53] and ultrasound-assisted methods.[54,55] No matter what method is used, it's paramount to ensure that there are no competing solvents that hinder the coordination. This is because the formation of CD-based MOFs is primarily driven by the coordination between metal ions and hydroxyl groups of CDs, although water molecules may also act as hydrogen bonding linkers between CDs or as ligands existing in the coordination sphere of metal ions.

The formation of CD-based MOFs is determined by the interaction between the hydroxyl groups and metal ions.

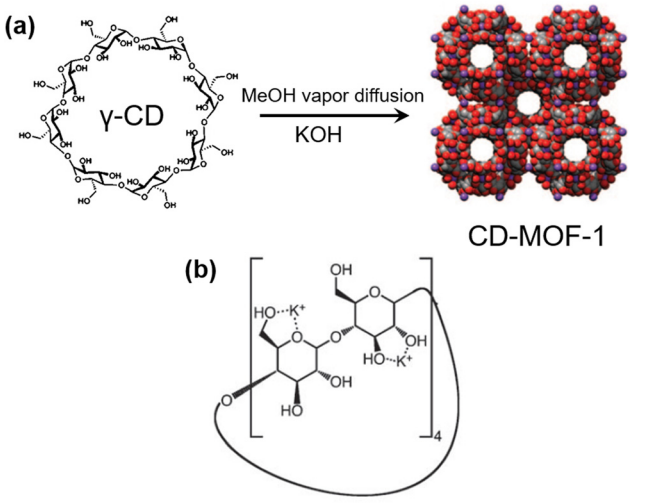

Fig. 2 (a) Preparation of γ-CD-K^+ MOFs using a vapor diffusion method. (b) The alternating coordination of K^+ ions to the primary and secondary face of a γ-CD.[22]

The –OCCO– motif can function as a bidentate coordinating arm to bind with metal ions (Fig. 2b). The 8-fold symmetry of γ-CD allows for the coordination of alkali metal cations to alternative α-1,4-linked D-glucopyranosyl residues, resulting in a cubic morphology with a space group of I432, whereas β-CD MOF and α-CD MOF crystallize in a monoclinic crystal structure with a space group of P21. Unfortunately, the coordination bond is relatively weak and vulnerable to water attack. Therefore, CD-based materials usually exhibit poor stability in humid and aqueous environments. In addition, CD-based materials also tend to harbor bacteria due to the sugar units in CDs. Therefore, these materials usually require additional protection.

2.1.2 Structure characteristics of CD-based MOFs. Distinct from MOFs composed of other organic linkers, CD-based MOFs form new topological networks that are rarely observed or predicted.[22] For instance, the first CD-based MOFs reported by Stoddart *et al.*, the γ-CD-K^+ MOF, consists of infinite body-centered frameworks of $(\gamma\text{-CD})_6$ cubic units linked by four K^+. The γ-CD units adopt the faces of a cube, with their secondary face pointing outward and their primary face inward. This arrangement forms a cubic void in the center with a diameter of 1.7 nm. In the $(\gamma\text{-CD})_6$ cubic units, γ-CDs are linked to one another by the coordination of four K^+ ions to the primary C6 OH groups and the glycosidic ring O atoms on alternating D-gluocopyranosyl residues on the γ-CD tori (Fig. 3a and b). These cubic $(\gamma\text{-CD})_6$ are then connected through K^+ coordination to the outward oriented C-2 and C-3 OH groups on the secondary faces of the other four D-gluocopyranosyl residues, adopting a body-centered cubic packing arrangement (Fig. 3c). Pores with a diameter of 0.78 nm defined by the γ-CD's tori propagate along three crystallographic axes and connect the cubic void, forming infinite channels.

Besides the cubic arrangement, a distinct class of framework structures has been generated by varying the types of CD and metal ions. In 2012, Stoddart reported a case of a CD-based MOF with a left-handed helical channel formed by α-CD and Rb^+ ions.[56] Intriguingly, in 2015, Lu *et al.* presented a new β-CD MOF with left-handed helical channels, which run through the structure created by the coordination of Na^+ to the primary and secondary faces of the β-CD rings[46] (Fig. 3d–f). These novel structures not only expand the diversity of CD-based MOFs but also have great potential for future applications.

2.1.3 Properties of CD-MOFs. By incorporating CDs into the periodic framework structure, CD-based MOFs exhibit properties that are not present in CD alone or simple CD complexes. This forms the basis for their innovative applications in drug delivery,[57,58] sensors,[59,60] gas storage and separation,[61,62] energy[63,64] and photochemistry.[65–67] The ability to accommodate substrates in pores, combined with their inherent chirality, enables them to facilitate regio- and stereoselective reactions. As an example, Stoddart and co-workers demonstrated the highly efficient (85% yield) [4+4] photodimerization of 1-anthracenecarboxylate (1-AC^-) under UV-light irradiation with excellent regioselectivity (91%) and good enantioselectivity (79% ee) by encapsulating 1-AC^- inside the cationic porous tunnels of γ-CD-K^+ MOF[68] (Fig. 4). By analyzing the crystal structure, they discovered that the substrate pairs are nanoconfined and aligned within the chiral extended framework of γ-CD-K^+ MOF. Moreover, K^+ ions serve as secondary recognition elements, stabilizing the relative orientation of the anionic 1-AC^- through attractive electrostatic interactions. Such unique properties of γ-CD-K^+ MOF, coupled with the inherent chirality of γ-CD, enable substrates to be packed in a highly oriented and asymmetrically nanoconfined space, resulting in exceptional regio- and stereo-selectivity.

Chirality and high emission efficiency are two prerequisites for luminophores to emit circularly polarized luminescence (CPL). In this regard, CD-based MOFs have proven to be a promising platform for constructing CPL materials. Firstly, the hierarchical porosity of CD-based MOFs allows them to

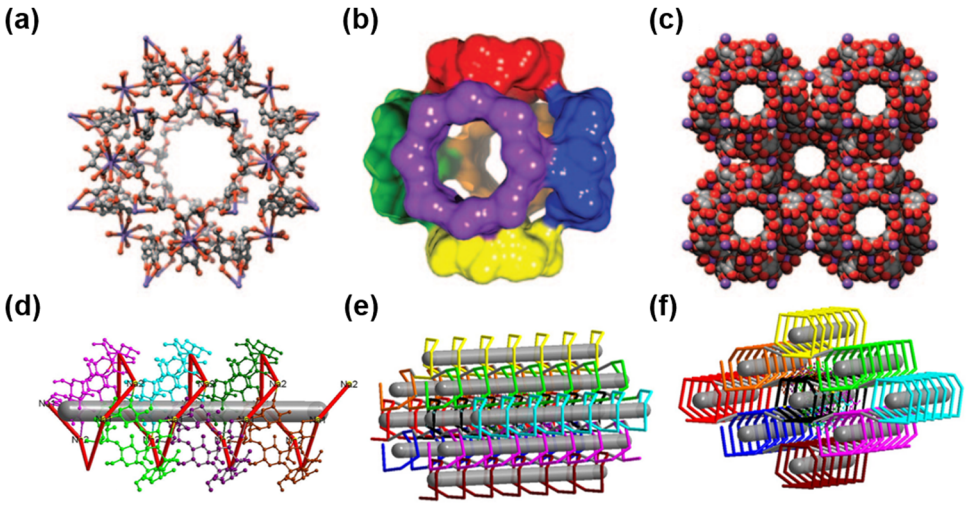

Fig. 3 (a) A ball-stick, and (b) space-filling representation of the cubic $(\gamma\text{-CD})_6$ repeating motif of CD-MOF-1. Six γ-CDs forming the six faces of the cube are shown in different colors. (c) Spacing-filling representation of the extended structure of CD-MOF-1.[22] (d) A ball-stick representation of 1D double chains in β-CD-MOF. (e) and (f) A schematic illustration of the topology of the 3D helical framework from different orientations.[46]

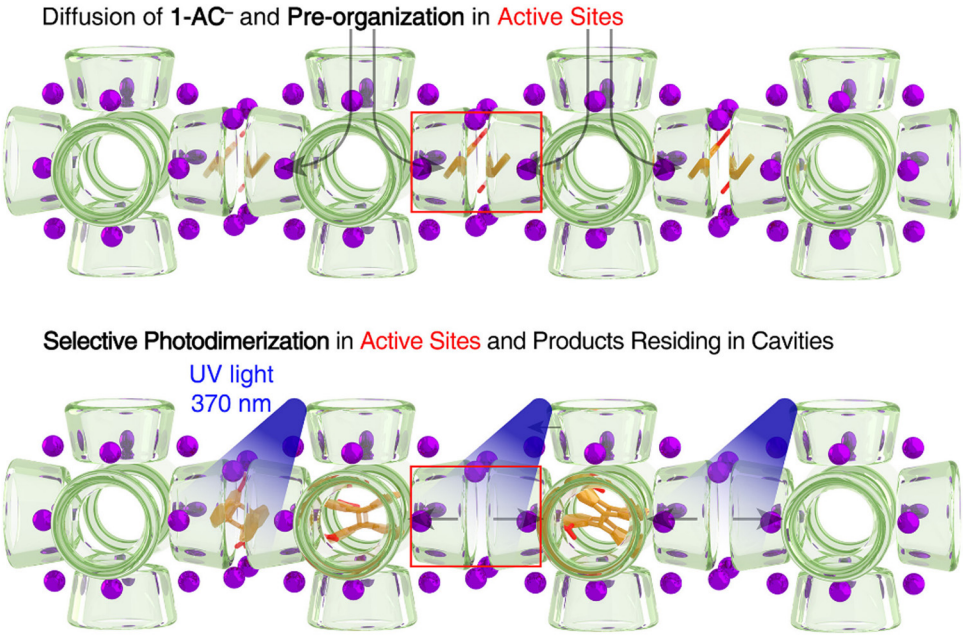

Fig. 4 Schematic representation of the photodimerization of 1-anthracenecarboxylate (1-AC$^-$) in γ-CD-K$^+$ MOF.[68]

accommodate a variety of luminophores, thereby significantly expanding the range of potential guests. Secondly, the nano-confined environment and crystalline structure are favorable for immobilizing molecules, which is a crucial requirement for efficient emissive materials.[65–67] Most importantly, CD-based MOFs could provide a chiral environment for luminophores, considering the chiral nature of CDs.[66] Circularly polarized luminescence (CPL) can be induced as achiral fluorescent dye is encapsulated either in the cavity of CDs or in the voids of the MOFs. For example, Liu *et al.* reported a series of efficient CPL materials based on γ-CD-K$^+$ MOFs.[66] By encapsulating luminophores that are much larger than the cavity size of γ-CD into the cubic void of γ-CD-K$^+$ MOFs *via* the *in situ* encapsulation strategy, CPL of the luminophores is induced (Fig. 5a). More intriguingly, the cubic void shows an interesting size effect (Fig. 5b). For a luminophore that is smaller in size than the cubic void but still larger than the cavity size of γ-CD, the interaction between the luminophore and the cubic void is not strong enough. As a result, the luminophore would be distributed at various positions within the cubic void. Therefore, the handedness of CPL is random and uncontrollable. In contrast, for a large one whose size matches well with the void, the luminophore would be well confined within the void, resulting in strong negative CPL signals. The cavity and void chirality of CD-MOF provides a versatile platform for fabricating crystalline CPL materials from either single AIEgens or ACQ luminophores, thanks to space confinement (Fig. 5c).

When CD coordinates with metal ions to form an extended three-dimensional framework structure, the overall conductivity of the composite is improved compared to the parent CD.[69] In addition, metal ions and hydroxyl groups can function as active sites for binding with the substrate and catalyzing reactions, making them good candidates for electrocatalysts. For example, Liu and co-workers utilized γ-CD-K$^+$ MOFs as a cathode material to achieve the NO^{3-} reduction reaction (NO^{3-} RR) under ambient conditions in an alkaline electrolyte[63] (Fig. 6a). They found that γ-CD-K$^+$ MOFs possess better electrocatalytic activity than the parent γ-CD, exhibiting a significantly higher NH_3 yield rate and faradaic efficiency. By conducting control experiments and in-situ characterization, the researchers attributed the better electrocatalytic activity to an enrichment effect in γ-CD-K$^+$ MOFs (Fig. 6b). Since the γ-CD-K$^+$ frameworks contain hydroxyl groups and K$^+$, the nitrate would be absorbed *via* hydrogen bonding and electrostatic interactions. Therefore, the frameworks act as nanoreactors filled with cages to initiate the NO^{3-} RR reduction reaction, thereby enhancing the performance of the reaction in an alkaline electrolyte.

Despite their numerous extraordinary properties, MOFs based on CDs still face significant challenges in practical applications. The most prominent one is their poor resistance to moisture and water. Because CDs are water-soluble, the CD-MOFs would disintegrate when exposed to a significant amount of water or high humidity. In addition, improving the resistance of CD-based MOF to bacteria is also of significance, as CDs are composed of sugar units that serve as excellent food sources for bacteria. To address these problems, various approaches have been attempted, including the rational design of ligands,[70] surface modification of MOFs,[71] cross-linking of CD units[50,72] and encapsulation of functional components.[73,74] In addition, constructing CD-based MOF hybrids or composites by integrating them with metal nanoparticles, biomolecules, or polymers would not only enhance the properties of native CD-MOFs, but also impart the materials with more promising functions.

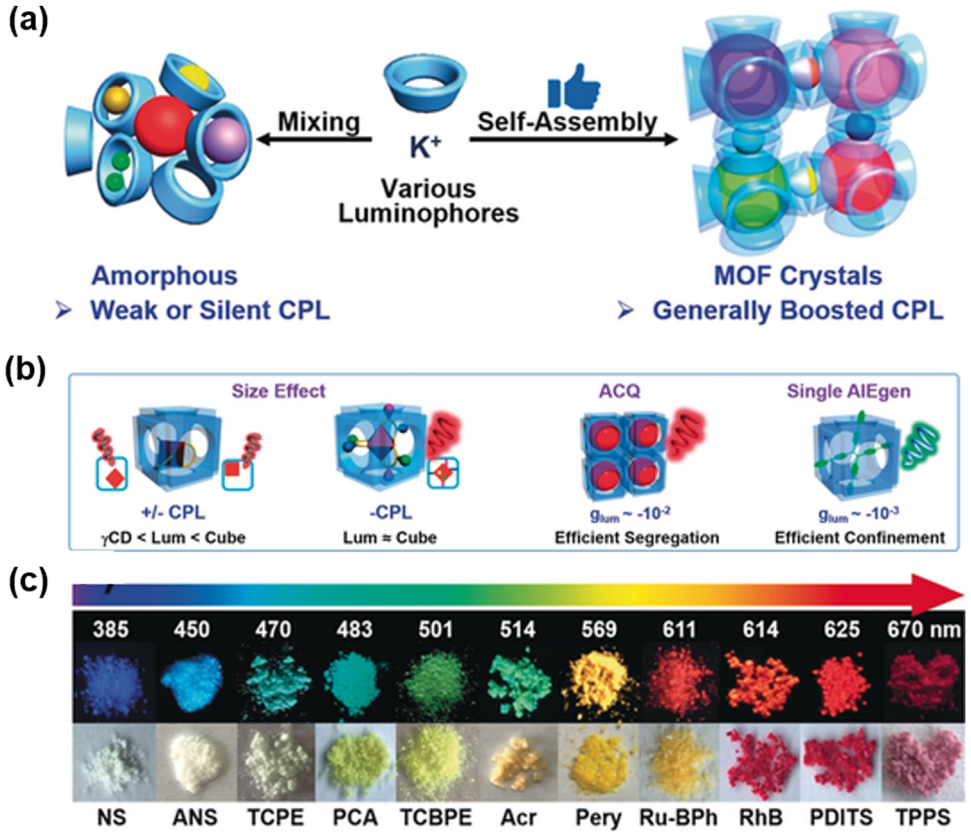

Fig. 5 (a) The mechanism of boosted CPL from lum@γ-CD-MOF and the size effect of CPL induction of ACQ and a single AIEgen based on cubic chirality. (b) Photographs of various CPL crystals of lum@γ-CD-MOF under the irradiation of 365 nm (upper) and visible light (lower).[66]

2.2 CD–POM based frameworks

Polyoxometalates (POMs) are polyanionic metal-oxygen clusters with a wide range of structural diversity and remarkable chemical and physical properties. They frequently act as building blocks for self-assembly.[75–77] To date, there have been few works reporting frameworks based on CD and POMs. Generally, the two components are bridged by metal ions, such as Na^+ and K^+, or they bind directly to each other *via* hydrogen bonding. In this section, we will discuss some examples of CD–POM based frameworks. Classified by the formation principles, CD–POM based frameworks can be divided into metal–organic frameworks (MOFs) and cluster-organic supramolecular frameworks (COSFs).

2.2.1 Structures of POM–CD MOFs. Considering the significant disparities between CD and POM, the reports on CD–POM-MOFs are still quite limited. The first case of POM–CD MOFs was presented by Khashab *et al.* They prepared the hybrid MOF *via* a facile solution technique, namely $[PW_{12}O_{40}]^{3-}$ (PW_{12}) and α-CD MOF (POT-CD)[25] (Fig. 7a). In the extended structure, K^+ and Na^+ cations bridge α-CD and PW_{12}. The coordination spheres of the metal ions are completed by oxygen atoms from the hydroxy groups of CD, terminal oxygens of PW_{12} and water. This arrangement forms a double layer with a certain offset distance. By sharing the metal sites between them, the double layers serve as the basic repeating unit and extend along the c-axis, resulting in a 3D framework (Fig. 7b). Notably, replacing POMs of different symmetry would lead to a distinct 3D framework called POP–CD (Fig. 7c and d). Their findings demonstrate that both POMs and CDs can serve as molecular building blocks, which can be effectively linked through coordination with metal ions.

2.2.2 Structures of POM–CD COSF. Apart from POM–CD MOFs derived from metal ion coordination, POM–CD hybrid frameworks can be constructed through hydrogen bonding between CDs and POMs. This leads to the emergence of cluster-organic supramolecular frameworks (COSFs). For example, Diao *et al.* reported the structure of POM–CD COSF (Fig. 8). CD units and Krebs-type $[Zn_2W_2]$ clusters are assembled together only through Na–O coordination bonds and hydrogen bonds, resulting in the formation of a three-dimensional open framework in $\{Zn_2W_2@2CD\}$.[24] They further employed the POM–CD COSF as a modified separator in Li–S batteries, which offers efficient trapping of lithium polysulfides (LiPSs) and catalytic sulfur redox on the cathode side.[24] In the hybrid, β-CD can capture the polysulfides through host–guest recognition and provide a Li^+ transmission channel, while the $[Zn_2W_2]$ cluster efficiently promotes the redox kinetics of the liquid/solid LiPSs–Li_2S conversion. The novel strategy leverages the host–guest chemistry and the catalytic nature of the functionalized framework to greatly enhance sulfur utilization and effectively mitigate the LiPS shuttling and Li dendrite growth.

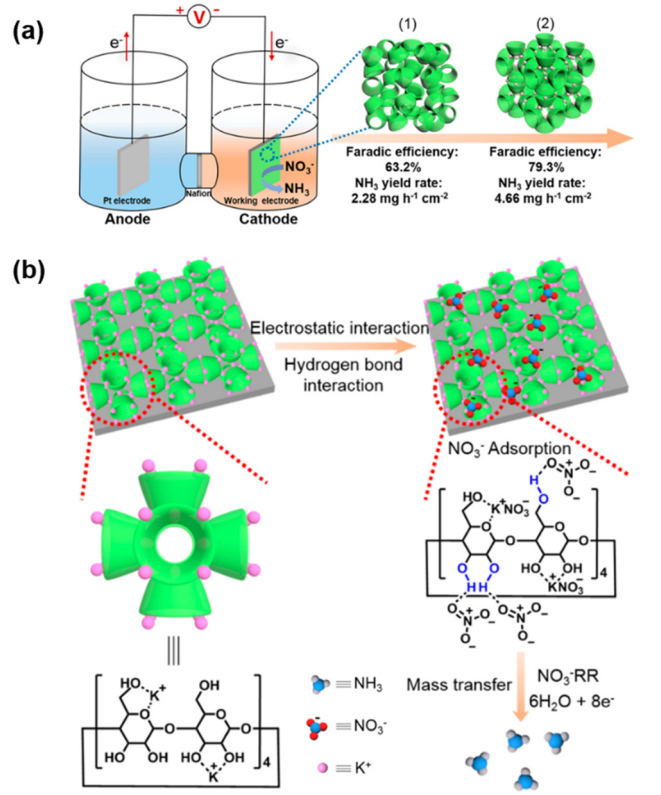

Fig. 6 (a) Schematic diagram of the electrocatalytic NO^{3-} RR for γ-CD and γ-CD-K^+ MOF in 0.1 M KOH/KNO_3 electrolyte. (b) Schematic illustration of the possible mechanism of the electrochemical nitrate reduction process catalyzed by γ-CD-K^+ MOF.[69]

This approach opens up new possibilities for exploring and designing POM–CD COSF with cutting-edge applications.

Cadot *et al.* prepared another case of POM–CD COSF by exploiting the affinity between chaotropic POMs and native CDs[23] (Fig. 9). The frameworks are constructed from infinite CD rod units decorated by the POM $[AlMo_6O_{18}(OH)_6]^{3-}$. These POMs interact with the outer walls of the CDs through hydrogen bonds formed between their hydroxyl groups. This bonding process glues two CD channels together, resulting in the formation of extended open frameworks. Notably, the rotational symmetry of CD dictates the topologies of the resulting supramolecular architectures, generating honeycomb and checkerboard-like networks for α-CD and γ-CD, respectively (Fig. 9a). The chaotropic effect of the low-charged polyanions is the primary driving force for the formation of these CD–POM frameworks. By utilizing the molecular recognition properties of the macrocycle units, these open supramolecular frameworks, which contain empty CD channels, could offer hosting space for capturing polyiodides[78] (Fig. 9b).

Plenty of studies have revealed that CD and POM can form POM@CD complexes, with the POMs positioned on the wider rim of the CDs.[79–81] The POM@CD complexes can then serve as secondary building units to assemble into a three-dimensional hybrid array. As an example, Zhan *et al.* reported two supercubic isostructures, Co/Cu-$PW_{12}O_{40}$-γ-CD.[26] The $PW_{12}O_{40}^{3-}$ trianion is encapsulated by γ-CD to form a POM@γ-CD entity *via* hydrogen bonding between the belt terminal O atoms of POM and the hydroxyl groups of γ-CD (Fig. 10a). Driven by coordination and hydrogen bonds, the $(POM@\gamma\text{-}CD)_{36}$ repeating motifs display a novel cage-in-cage configuration $\{(POM@\gamma\text{-}CD)_{12}\}@\{(POM@\gamma\text{-}CD)_{24}\}$, adopting a super cubic packing arrangement (Fig. 10b and c). Notably, the redox properties of the POM encapsulated in the CD are largely retained, and additional electrochemical stabilization is observed.

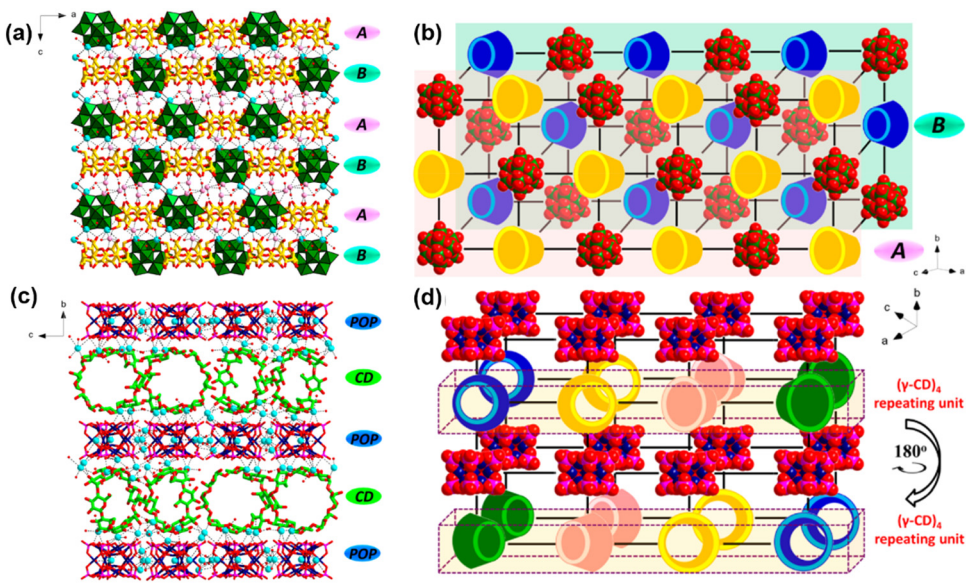

Fig. 7 (a) Combined polyhedral/ball-and-stick representation of POT–CD. Color code: WO_6, green octahedra; PO_4, pink tetrahedra; K, turquoise; Na, magenta; O, red; C, yellow. (b) A schematic representation of the double-layer repeating unit. (c) A ball-and-stick representation of POP–CD. Color code: Pd, blue; P, pink; K, turquoise; O, red; C, green. (d) A schematic representation of the $(\gamma\text{-}CD)_4$ repeating unit.[25]

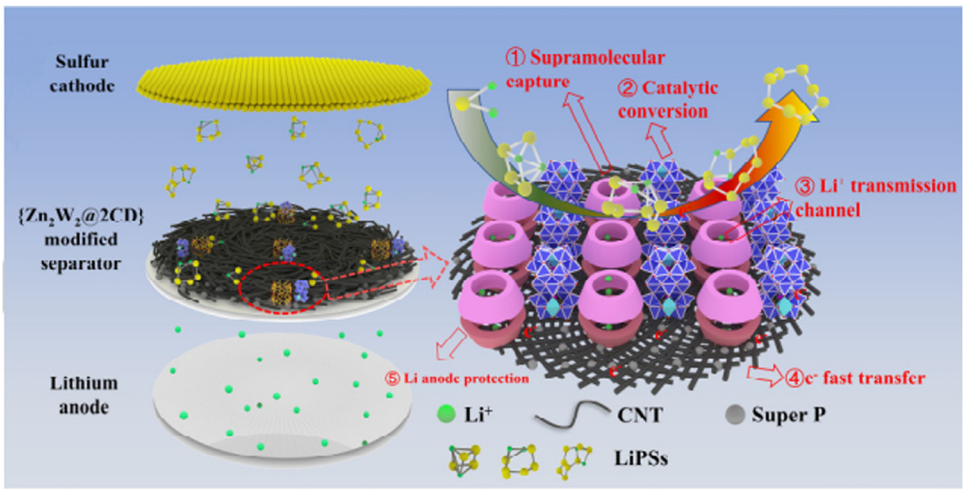

Fig. 8 Schematic illustration of the working principle and configuration of the LSBs with this {Zn_2W_2@2CD} modified separator.[24]

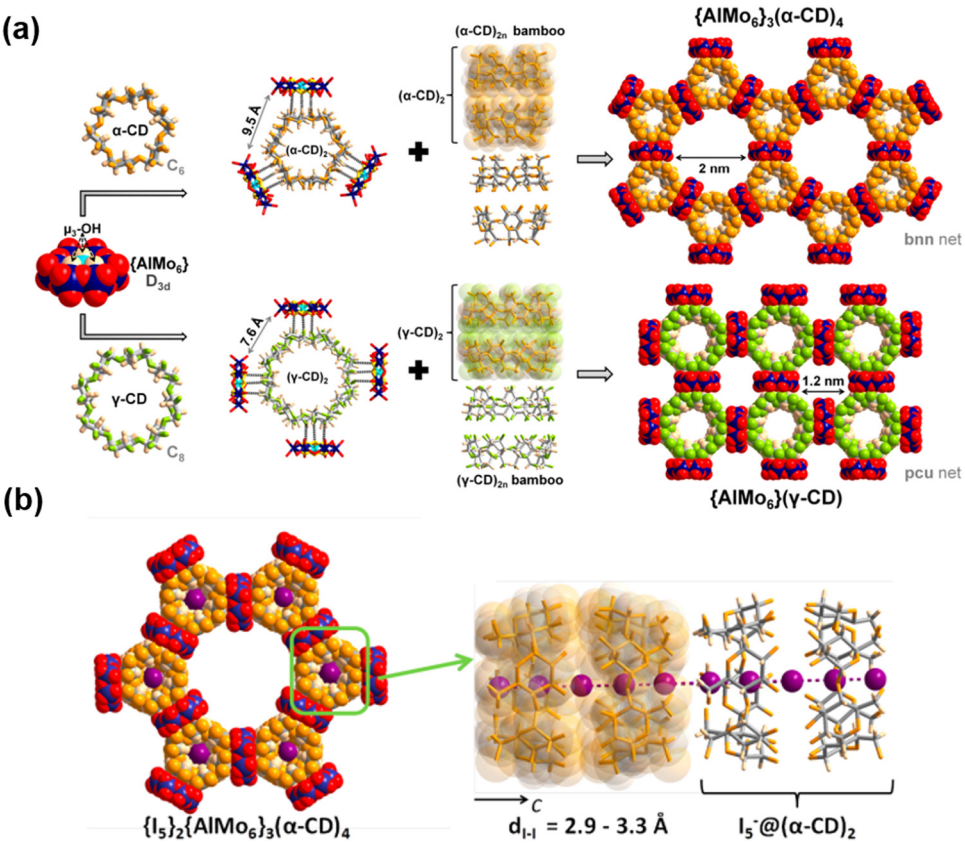

Fig. 9 (a) The structural arrangements of {$AlMo_6$}$_3$(α-CD)$_4$ (top) and {$AlMo_6$}(γ-CD) (bottom) with distinct topologies. (b) Concentration of I^{3-} in an aqueous solution after the addition of Na_3{$AlMo_6$} and representation of the crystal structure of {I_5}$_2${$AlMo_6$}$_3$(α-CD)$_4$.[23]

3 CD-based crystalline self-assembly

For a long time, CDs were viewed as a disruptor for amphiphilic assembly. For example, a CD can destroy the assembled structures of surfactant micelles,[82–84] lipid vesicles[85] and the complexes of surfactants and biomacromolecules such as DNA[86] and proteins.[87] CD's destruction over assembly arises from the hydrophilic nature of CD, which would boost the water solubility of guests through complexation, thereby undermining the hydrophobic effect that facilitates the assembly. However, an increasing number of studies have shown that the abundant hydroxyl groups in CDs can play a significant role

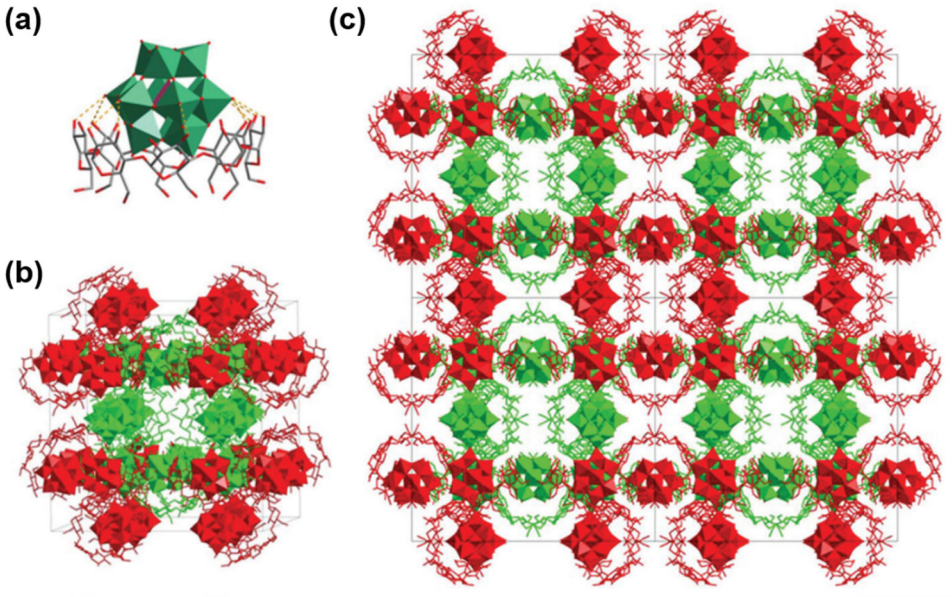

Fig. 10 Structural representations of (a) POM@γ-CD directed by hydrogen bonds. (b) {(POM@γ-CD)$_{12}$}@{(POM@γ-CD)$_{24}$} in a cell. (c) The stacking pattern of cubes in a cage-in-cage manner. POMs: polyhedra, CDs: wires.[26]

in self-assembly. As an example, the polypseudorotaxanes based on α-CD and PEG could generate a supramolecular hydrogel.[88–90] The self-assembled crystalline complexes, which are held together by hydrogen bonds between CDs, can function as physical network knots and initiate gelation. In the last decade, numerous new molecular assemblies based on hydrogen bonds between CDs have been reported. Specifically, crystalline self-assemblies have been extensively studied and reported.

3.1 Formation principle of crystalline self-assembly

Crystalline self-assembly was firstly observed in β-CD-surfactant systems[27,28,91–94] and gradually expanded to other β-CD-guest systems, including alkane,[95,96] aromatic hydrocarbon[97] and amine.[98] Guests are firstly included into the CD cavity, generating host–guest complexes in solution. Then, the host–guest complexes would further assemble into high-order structures dominated through hydrogen bonds between CDs. In contrast to traditional amphiphilic assemblies, which are often soft and fluidic, crystalline self-assembly is found to be very rigid and robust.

Among the three native CDs, β-CD is the most extensively used when constructing crystalline self-assemblies. This is due to its relatively low water solubility, which allows the complexes to readily form assemblies in water. Although the crystalline self-assembly is primarily dominated by interactions between CDs, the surfactants hosted in their cavities also play an important role in modulating the assembly. When there is no additional repulsive force between the surfactant head groups, the hydrogen bonds between CDs can cause precipitation at high concentrations. However, when there is repulsion that undermines the strong hydrogen bonds between CDs, such as the electrostatic repulsion between the head groups of charged surfactants, the assembly will remain dispersed in water even at very high concentrations.

3.1.1 Crystalline self-assemblies based on CDs and surfactants. The first case of crystalline self-assembly was based on the anionic surfactant sodium dodecyl sulphate (SDS) and β-CD.[27] One SDS molecule is included with two β-CD molecules, forming SDS@2β-CD complexes (Fig. 11a). The SDS@2β-CD units then assemble into multiwalled microtubes through hydrogen bonds between β-CDs. Further tests indicated that the self-assembling behavior of SDS@2β-CD in water is concentration-dependent.[91] As the weight concentration increases from 4% to 50%, vesicles, multiwall microtubes, and lamellae are obtained, respectively[91] (Fig. 11b). It is noteworthy that the 'vesicles' were later confirmed to have 12-faced rhombohedral crystalline self-assembly[94] (Fig. 11c). The strong, directional in-plane hydrogen bond between CDs and the out-of-plane repulsion resulting from the head groups of SDS work synergistically to impart structural rigidity and in-plane crystallinity to the self-assembly.

This crystalline self-assembly can be generalized in other β-CD/surfactant systems.[27,28,91–94] Regardless of anionic $SDSO_3$ and SDBS, cationic CTAB, zwitterionic TDPS, and nonionic Tween 20, all of these surfactants can form crystalline assemblies with β-CD at appropriate concentrations. Because the repulsion effects brought about by surfactants vary, the specific structures and concentration ranges required to achieve these structures also differ.

3.1.2 Crystalline self-assembly based on CDs and alkane. Since crystalline self-assemblies are mainly driven by hydrogen bonds between CDs, the hydrophilic portion of the surfactant merely regulates the strength of interaction between neighboring CDs. Zhou *et al.* then considered replacing surfactants with alkanes.[95,96] As the liquid alkane dodecane was used instead of

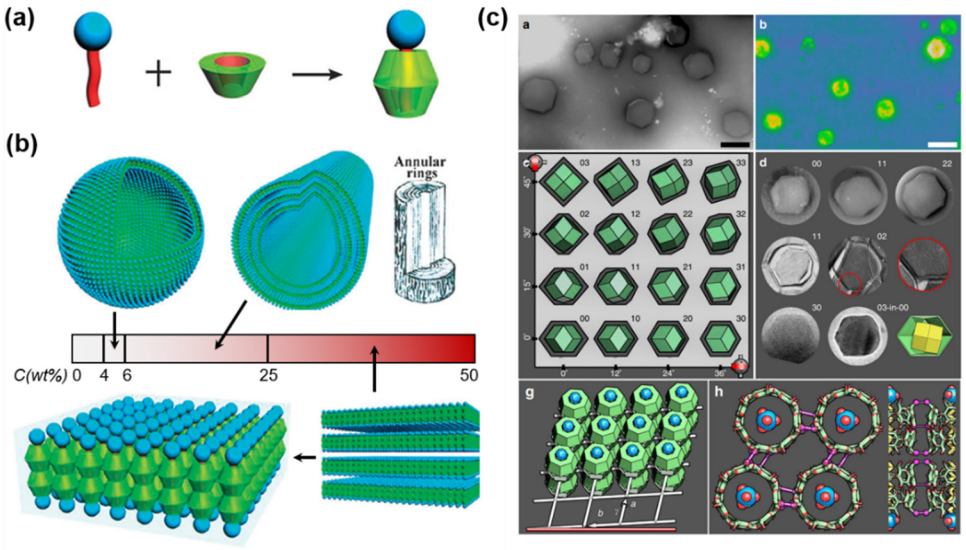

Fig. 11 (a) SDS@2β-CD complexes. (b) A schematic showing the self-assembly behavior of SDS@2β-CD at different concentrations.[27] (c) The morphology of the SDS@2β-CD polyhedral and views of the in-plane lattice of SDS@2β-CD crystalline assembly.[94]

SDS, the dodecane@2β-CD units formed again and subsequently self-assembled into well-defined vesicles or bricks, depending on the concentration. At low concentrations, a greater number of water molecules are involved in the formation of vesicles. In contrast, at high concentrations, β-CD dimers are able to closely pack together through intermolecular hydrogen bonds, resulting in the formation of planar self-assemblies.

Considering that self-assembly can be significantly impacted by subtle structural differences in the building blocks, guests with different geometrical shapes would affect the crystalline assembly and exhibit distinct self-assembling behavior and structure. For example, we reported that three xylene isomers@α-CD complexes have distinct assembly morphologies[97] (Fig. 12a). Due to the asymmetry of the wider and narrower rims of a CD, three isomers have different orientations in the CD's cavity. In detail, *o*-xylene is able to thread into the cavity of α-CD, with the two methyl groups accommodating at the wider rims of α-CD to decrease steric hindrance. In contrast, *m*- and *p*-xylene would thread into CD's cavity with no preferred direction. When these host–guest complexes further assemble into a crystalline assembly driven by the hydrogen bond between CDs, the different host–guest conformations are reflected in distinctly different self-assembly morphologies. Since the outcropping *o*-xylene hinders the formation of a hydrogen bond along the direction vertical to the α-CD symmetry axis, *o*-xylene/α-CD complexes are connected through hydrogen bonds along the α-CD axis, resulting in the formation of nanofibers with a high aspect ratio. For complex assemblies with *p*- and *m*-isomers, much shorter ribbons and bricks are formed, which fail to gel water and phase separate from the system (Fig. 12b and c).

3.1.3 Application of the crystalline self-assembly of CDs. Owing to the temperature sensitivity of hydrogen bonds, the crystalline self-assembly is responsive to temperature changes. For example, we reported the reversible transition between SDS@β-CD microtubes and vesicles triggered by temperature.[93] On that basis, Jiang *et al.* found that colloidal particles are able to co-assemble with the microtubes and be incorporated inside the microtubes during the cooling-down process[99] (Fig. 13a). More intriguingly, depending on the size of the particles, colloidal particles have shown various packing patterns inside the microtubes, including linear, helical, zig-zag, and zipper configurations (Fig. 13b). If the particles are much smaller than the tube diameter, there will be no preference for their distribution inside or outside the tubes, and they will be randomly distributed. This research discloses that the self-assembled structure is closely related to the space effect. It clearly demonstrates that the interplay between molecular and colloidal self-assembly could lead to new possibilities for creating innovative functional materials.

3.2 Chirality controllable self-assembled materials based on the crystalline self-assembly of CDs

CDs are chiral and enantiomerically pure. It has long been observed that achiral guests show induced circular dichroism (ICD) signals when included in a CD cavity. The sign of the ICD signal can be accurately predicted by Harata–Kodaka's rule.[100–102] If the electric dipole transition moment (μ) of the included guest is parallel to the CD's cavity axis and the moment center is inside the CD cavity, the ICD signal would be positive.[100,101] If the moment center is outside the CD cavity, the ICD signal is negative. However, if μ is perpendicular to the cavity axis, all the ICD signals above are reversed. Although Harata–Kodaka's rule has provided a clear understanding of the induced chirality of guests and served as a convenient tool for estimating the conformation of CD complexes,[103] it hadn't been applied in the field of chiral materials until the

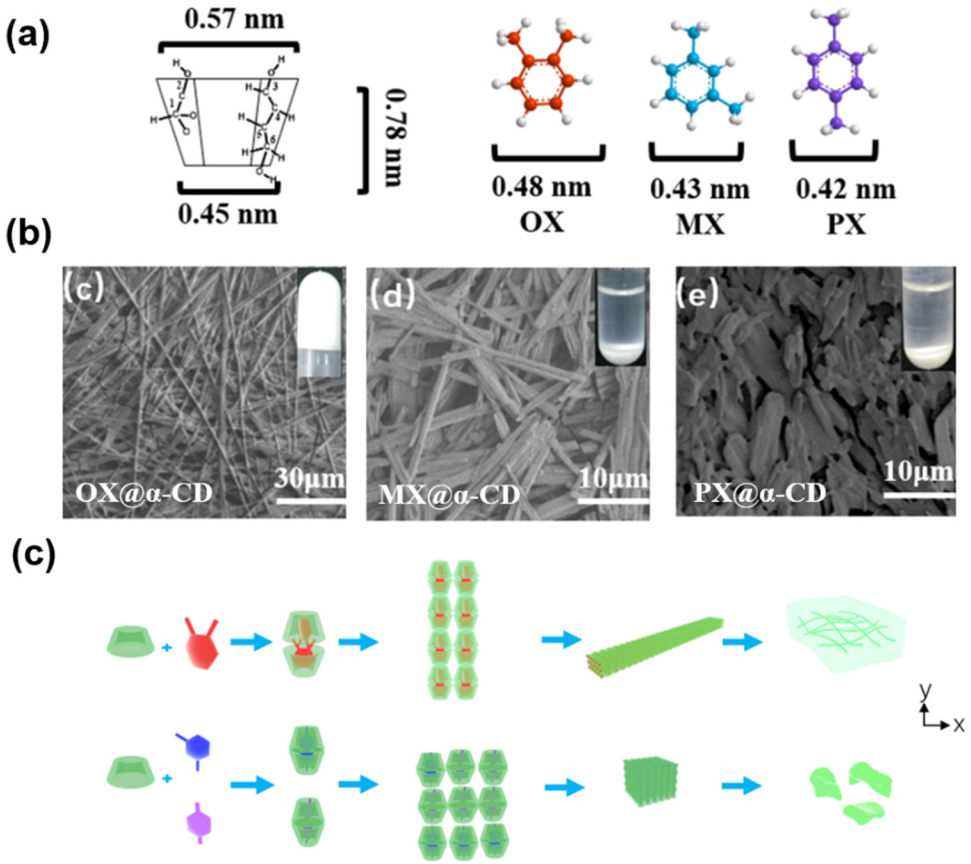

Fig. 12 (a) Schematic structures and molecular dimensions of α-CD and xylene isomers. (b) Photographs and SEM images of three xylene isomers@α-CD complex assemblies. (c) A schematic diagram of the possible self-assembly route in the xylene isomers@α-CD complexes.[97]

development of crystalline self-assembly.[104] Since discrete host–guest complexes do not have fixed orientations in solution, the electric dipole transition moments of the guests would cancel each other out. However, when discrete host–guest complexes organize into crystalline self-assembly, the guests are orientated orderly, which is favorable for enhancing a chiral signal. More importantly, due to the dynamic nature of crystalline self-assembly, chirality can be easily manipulated facilely by adjusting environmental factors, such as temperature, concentration, and host-to-guest ratios. Therefore, the crystalline self-assemblies are undoubtedly very promising for creating supramolecular materials with controllable handedness.

3.2.1 Chiral crystalline self-assembly. Wang *et al.* constructed the first chiral crystalline self-assembly using β-CD and alkyl amines.[98] They found that C8 and C9 alkyl amines can form helical crystalline structures with opposite circular dichroism signals (Fig. 14a). In detail, the circular dichroism signal for the C8 system is positive, while that for the C9 system is negative (Fig. 14b). The opposite chiral signals arise from different relative locations of the NH_2 group within β-CD's cavity. Since the C8 chain is shorter than the C9 chain, the center of the electron transition dipole moment for the C8 alkyl amine is located inside the CD cavity, whereas the center for the C9 amine is located outside of the CD cavity. Inspired by the chain-length dependent chirality inversion, the authors manipulated the handedness of the self-assembled crystalline materials by controlling the host–guest dynamics, in order to control the relative location of guests in the cavity (Fig. 14c). For fast exchange between guests inside and outside the CD cavity, the guest will be shallower in the cavity, while the center of the electronic transition dipole moment center will be located outside the cavity. This arrangement results in a negative circular dichroism signal, in accordance with Harata–Kodaka's rule. In contrast, a slower guest exchange would lead to deeper threading, thus generating a positive chiral signal. Using this principle, they can manipulate the handedness of the self-assembled materials by controlling the host–guest dynamic through modulation of concentrations and the molar ratio between the amines and CD. Considering that the enzyme will hydrolyze CD and subsequently increase the molar fraction of amines, an enzyme-responsive chirality inversion was also created.

3.2.2 Crystalline self-assemblies with controllable CPL handedness. By co-assembling with luminophores, the crystalline self-assembly based on CD is very promising for creating CPL materials. For example, Jiang and Duan *et al.* disclosed the hierarchical chirality transfer from CD, *via* CD complexes, to the final microtubes in the SDS@2β-CD system. On this basis, by simply doping the fluorescent dyes ThT and NR, the

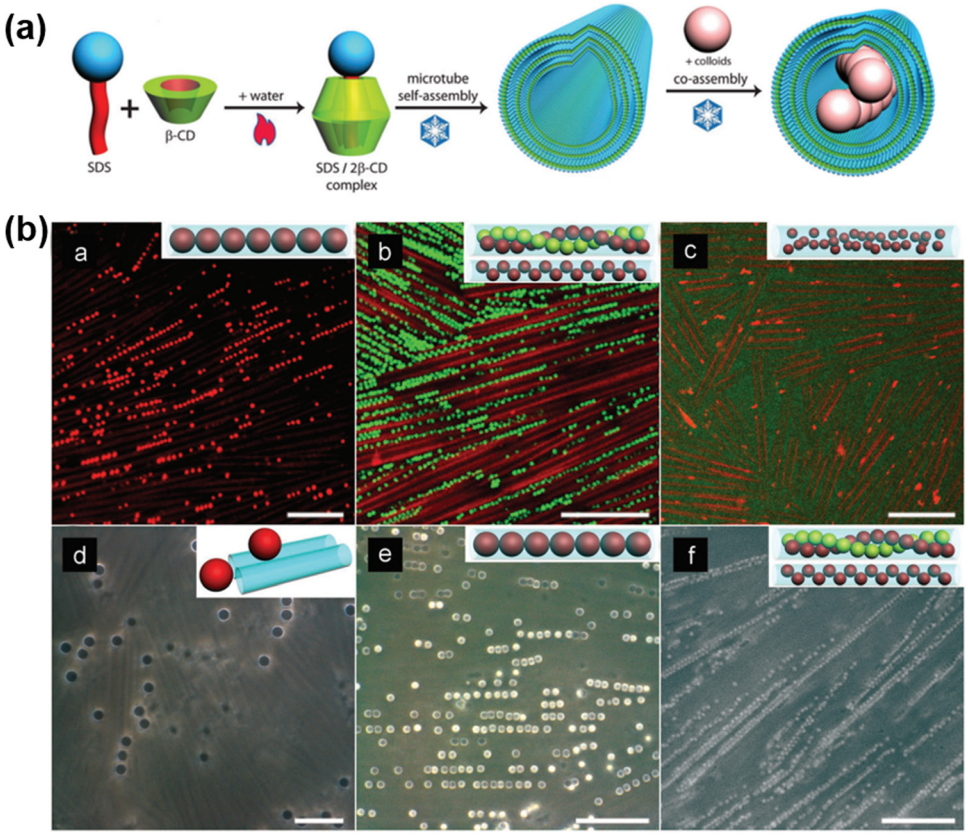

Fig. 13 (a) Representation of the self-assembly of SDS@2β-CD inclusion complexes into microtubes, incorporating and structuring spherical colloids in their cylindrical cavities. (b) Size-dependent arrangement of colloidal silica and polystyrene (PS) spheres in microtubes revealed by CLSM (upper) and optical microscopy images (lower).[97]

supramolecular chirality of the microtubes would transfer to the co-assembled dyes, enabling a strong left-handed CPL.[38] Wang *et al.* took a step forward in manipulating the handedness of the CPL in this system by controlling temperature[105] (Fig. 15a). As microtubes disassemble upon heating, unoccupied CDs become available to encapsulate ThT. Since the extended length of ThT is longer than the depth of CD, the electronic transition dipole moment center of the dye falls outside of the CD cavity. This results in a negative induced chiral signal, corresponding to right-handed CPL. Therefore, the CPL handedness can be precisely manipulated by carefully controlling temperature and is completely reversible (Fig. 15b).

4 CD-catalyzed assembly

A high affinity is favorable for host–guest complex formation. However, CD complexes generally have a low binding affinity, especially when compared to cucurbituril.[106–109] For example, Houk *et al.* reported that the average binding affinity for α-, β-, and γ-CD complexes ($K_a = 10^{2.5\pm1.1}$) is an order of magnitude smaller than the corresponding value for cucurbituril complexes ($K_a = 10^{3.4\pm1.6}$).[110] This weak binding feature renders CD another role that has long been ignored, namely, modifying the dynamics of self-assembly of the guest. This is especially true for guests with poor water solubility. In this case, CD complexes would work as intermediate and transient components to regulate the assembly pathway of the guest molecules and generate diverse assembled structures that cannot be achieved through conventional methods. In this section, we will discuss cases where CD acts as a "catalyst" to impact the assembly process but does not participate in the final assemblies.

4.1 Morphology modification

Given that CDs have a hydrophobic interior and a hydrophilic exterior, CDs can greatly enhance the water solubility of guest molecules through inclusion. Therefore, introducing CD to an amphiphilic assembly system may generate strong competition between hydrophilic and hydrophobic effects. Therefore, complexation can be employed to slow down the aggregation or precipitation of strongly hydrophobic molecules (Fig. 16a). For instance, the amphiphilic terthiophene compound TTC4L quickly precipitates at acidic pH, resulting in an amorphous structure. In contrast, when TTC4L molecules were encapsulated into β-CD, the precipitation upon acidification was obviously retarded and well-defined microspheres were formed[31] (Fig. 16b). Intriguingly, the microspheres were found to be composed of protonated TTC4L, and no β-CD was involved. The distinct morphologies suggest that the inclusion

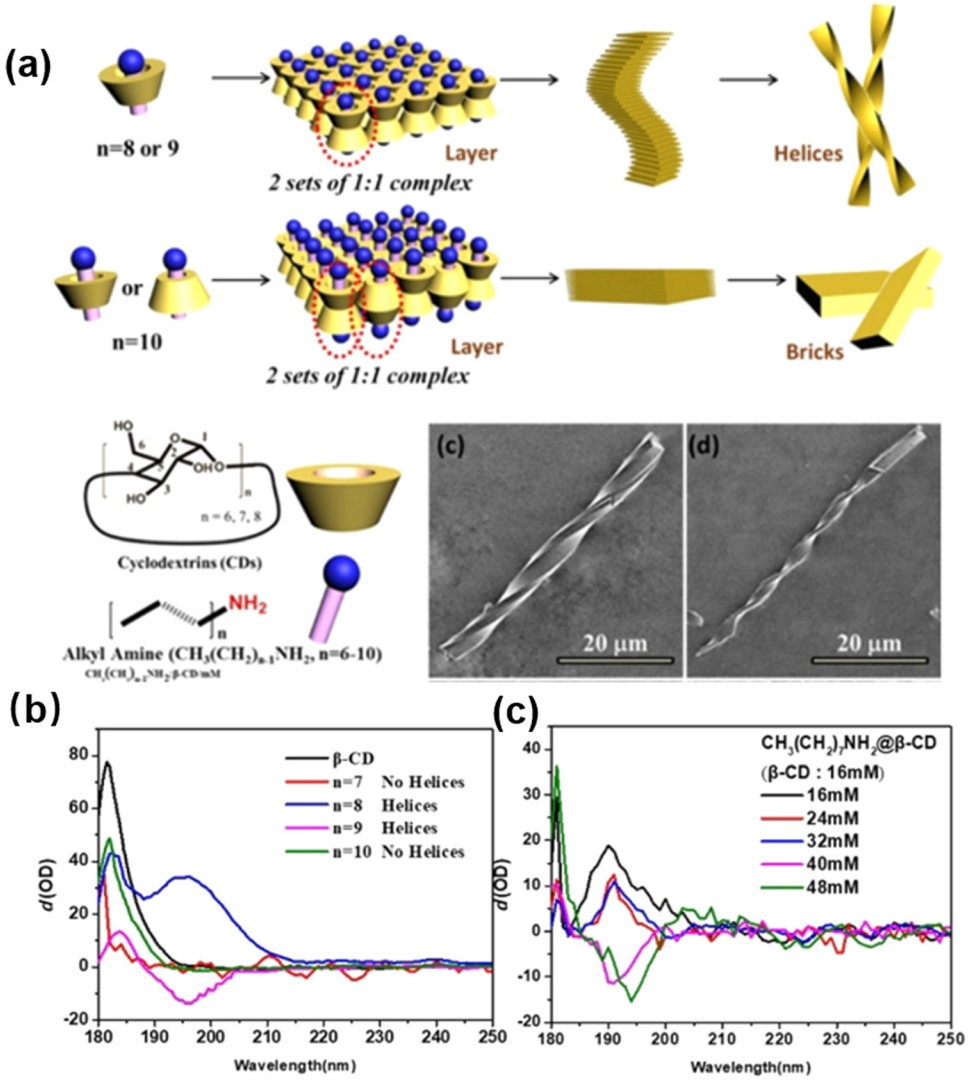

Fig. 14 (a) Schematic illustration of the mechanism of the formation of distinct assembly structures arising from different orientation of amines embedded in the cavity. (b) Circular dichroism spectroscopy of CH_3–$(CH_2)_{n-1}NH_2$@β-CD (n = 7–10) systems, (c) $CH_3(CH_2)_7NH_2$@β-CD systems with increasing the concentration of $CH_3(CH_2)_7NH_2$ at a fixed concentration of β-CD.[98]

of TTC4L into the cavity of β-CD has significantly altered the amphiphilic assembly of TTC4L upon acidification. As the free TTC4L molecules in solution are consumed upon acidification, the host–guest complex of TTC4L@β-CD would shift towards dissociation, releasing TTC4L molecules into solution. Consequently, the concentration of free TTC4L in the solution remains at a constant low level, and the precipitation kinetics are significantly slowed down.

A similar ''catalyst'' role of CD in modulating the assembly pathway was also observed in the coordination-triggered assembly of 1-pyrenebutyrate(1-PBA)[32] (Fig. 17a). The coordination-driven assembly between Zn^{2+} and 1-PBA occurs rapidly in a disordered manner, resulting in the formation of amorphous, sheet-like precipitates. However, by pre-including 1-PBA into γ-CD and adding Zn^{2+} to the 1-PBA@γ-CD solution, a well-defined microflower assembly is generated (Fig. 17b). The microflower assembly has exactly the same composition and molecular arrangement as the amorphous one, which is made up of stacked layers of two 1-PBA molecules bridged by one Zn^{2+}. Control experiments by replacing γ-CD with smaller α, β-CD, which cannot accommodate 1-PBA, only resulted in the formation of amorphous precipitates. As 1-PBA is threaded into the cavity of γ-CD, the stacking of 1-PBA triggered by Zn^{2+} coordination is not as easy as in the γ-CD-free system. Additionally, the smaller flakes tend to integrate into microflowers to minimize the surface energy to the maximum extent possible.

4.2 Chirality regulation

Besides modifying assembly morphology *via* pre-inclusion, we found that CD can induce symmetry breaking in a coordinating assembly system[33] (Fig. 18a). In the absence of α-CD, Zn^{2+} and alkyl azobenzene carbonate (C4AZO) would assemble into racemic cone shells with no discernible circular dichroism

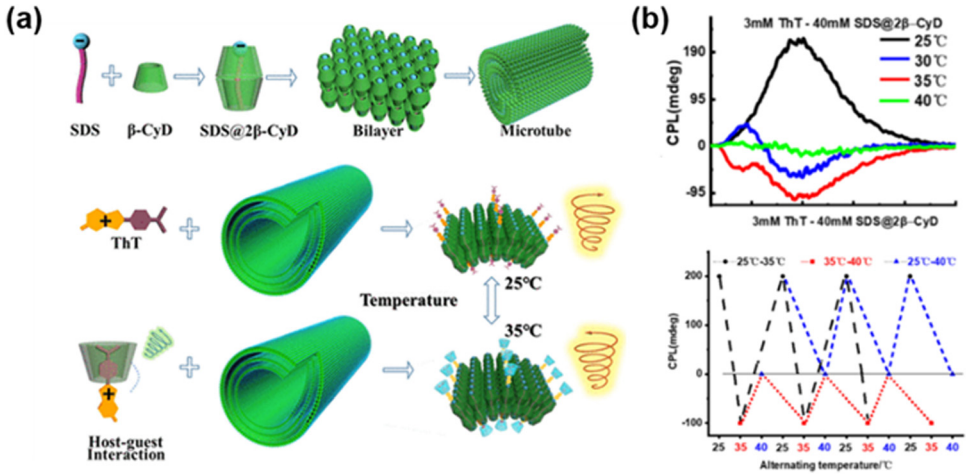

Fig. 15 (a) The co-assembly of fluorescent dye ThT with the microtube formed by crystalline assembly of SDS@2β-CD with temperature-triggered CPL inversion. (b) CPL spectra at different temperatures (upper) and switchable CPL inversion cycles (at 590 nm) by alternately changing the temperature.[105]

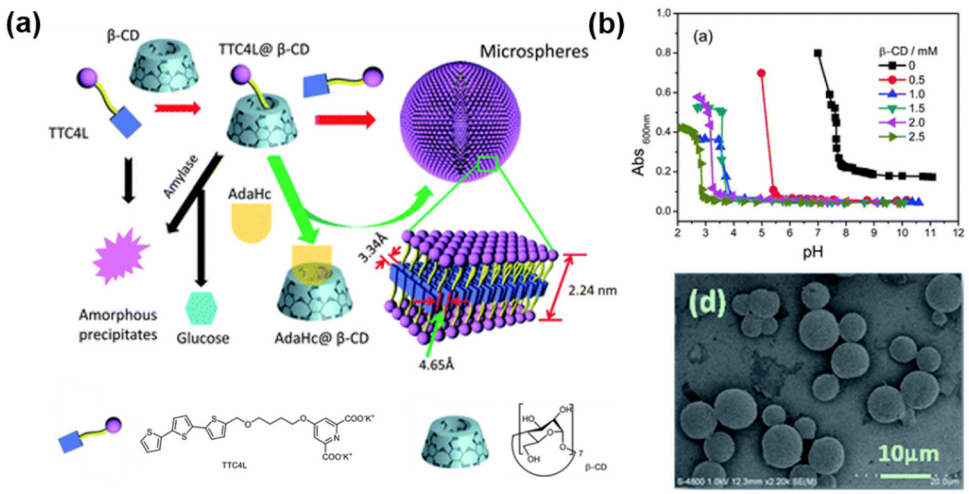

Fig. 16 (a) Proposed mechanism of the CD catalyzed molecular self-assembly of TTC4L into microspheres. (b) Turbidity curves of TTC4L@β-CD complex systems at various concentrations of β-CD under different pH and SEM images of the precipitates formed in the TTC4L@β-CD systems upon acidification.[31]

signal. In contrast, when C4AZO was allowed to form a host–guest complex with α-CD at a molar ratio of 1:1, the chiral cavity of α-CD could induce a chiral signal for the achiral C4AZO. In this case, the coordination assembly driven by Zn^{2+} was dominated by right-handed chiral cone shells, and the system exhibited a distinct circular dichroism signal. In other words, α-CD's inclusion has "catalyzed" the symmetry breaking of a coordinating assembly that would otherwise be racemic. Upon the addition of Zn^{2+}, the coordination interaction reduces the electrostatic repulsion between C4AZO molecules. As a result, π–π stacking is significantly promoted and α-CD is squeezed out of the system, thereby leaving the chirality of the supramolecular complex to the coordinating assembly of $Zn(C4AZO)_2$. More intriguingly, by controlling host–guest dynamics through varying temperature, concentration, or host–guest molar ratio, different complex conformations can be generated. This allows for the selective formation of either left- or right-handed $Zn(C4AZO)_2$ cone shells, and the chiral signal of the system can be rationally manipulated (Fig. 18b).

5 Summary and perspectives

In the present review, we summarize the new opportunities for CDs in supramolecular self-assembled materials, including the formation of MOFs, crystalline self-assembly, and catassembly. CDs can function as molecular building blocks, assembling with metal ions to construct CD-based MOFs. The hierarchical porosity and nanoconfined void, combined with their high crystallinity, make them an excellent platform for accommodating various substrates and performing specific functions in

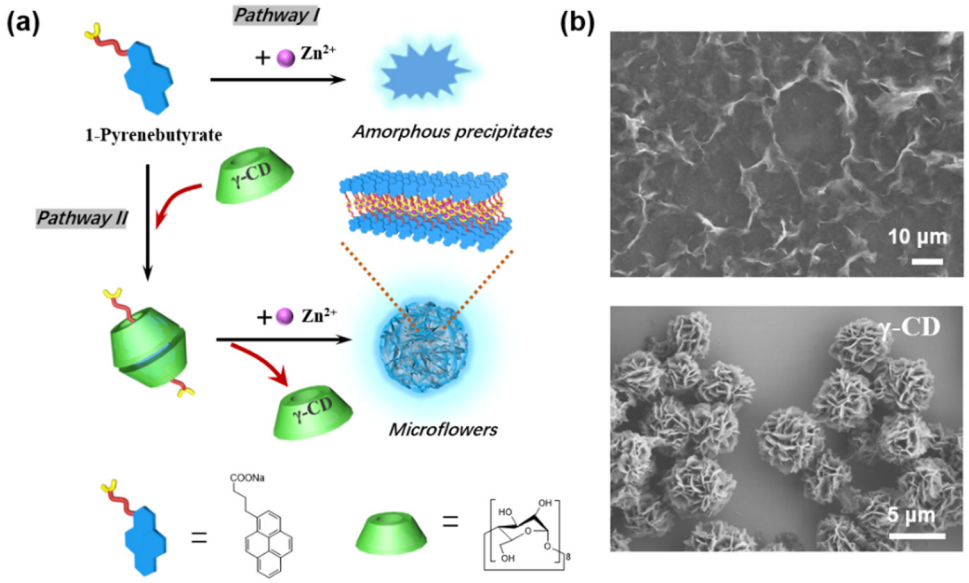

Fig. 17 (a) Schematic drawing of the proposed mechanism of γ-CD-catalyzed molecular self-assembly of 1-pyrenebutyrate and Zn^{2+} into microflowers. (b) SEM images of the precipitates obtained without CD (up) and in the presence of γ-CD (down).[32]

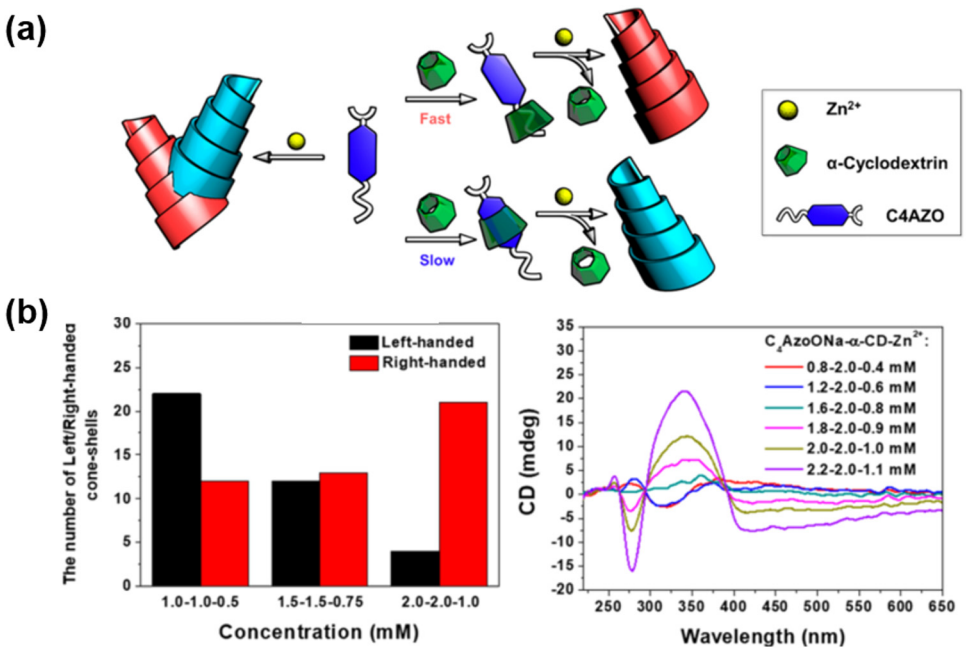

Fig. 18 (a) Proposed mechanism of α-CD-catalyzed symmetry breaking in racemic cone-shell self-assemblies. (b) Regulation of assemblies' handedness *via* modulating kinetic factors like concentration and molar ratio.[33]

photocatalysis, energy storage, and CPL materials. When considering practical applications, the post-modification or fabrication of CD MOF hybrids and composites with other functional components would effectively address the limitations of native CD-based MOFs. These limitations include poor resistance to water and bacteria. Apart from metal ions, CDs can integrate with POMs to build framework structures through coordination or hydrogen bonds. For the future, there are still many possibilities for incorporating CDs into hybrid materials. Much effort should be devoted to seeking new methods to integrate various inorganic components (*e.g.*, quantum dots, metal nanoparticles, and metal clusters) with CD and exploring their potential applications in various fields. The challenges are significant, given that integrating these completely dissimilar building blocks into a cohesive system is difficult, and the relationship between structure and property is often unclear. Despite the great challenges, the combination of CD and inorganic components through a supramolecular assembly strategy would undoubtedly imbue the hybrid materials with the inherent functions of inorganic materials, while also

providing the excellent reversibility and responsiveness inherent in supramolecular assembly.

Distinct from traditional amphiphilic assembly, which is mainly driven by hydrophobic interaction, crystalline self-assembly is dominated by hydrogen bonds between CDs. Due to the formation of an in-plane lattice arrangement held together by hydrogen bonds, these crystalline assemblies feature high rigidity and crystallinity, which are in high analogy with protein assembly in nature. Based on the crystalline self-assembly, the scenarios of Harata–Kodaka's rule can be well demonstrated, and this can be further applied to construct controllable chiral materials. Although crystalline self-assembly has been thoroughly examined, there are still ample opportunities for further exploration, particularly in relation to its potential in constructing chiral materials. In addition, crystalline self-assembly can serve as a valuable platform for investigating fundamental phenomena, thanks to its well-defined structure–property relationship. More advanced applications can also be envisioned by replacing the non-functional guest with another functionalized one. However, it should be noted that it still remains a significant issue when it comes to the practical application of various CD-based self-assembled materials. CD can be easily fractured by acid because the acetal linkages that join the sugar units are sensitive to acid. In addition, the CD MOFs are also not resistant to bacteria. Usually, the aqueous systems of various CD inclusion compounds cannot be preserved for a long time without specific antibacterial protection.

Besides serving as basic building blocks for the final assembled structures, the inclusion of CDs greatly alters the assembly pathway of the embedded guests, leading to CD-catalyzed assembly. In this sense, CDs work as a ''catalyst'', only functioning during the intermediate assembly pathway and not contributing to the final assembly. By incorporating the guests into the cavity beforehand, well-defined microspheres and microflowers are formed in the modified assembly pathway, while only amorphous precipitates are generated through the direct assembly pathway. Apart from modifying assembly's morphology, CD pre-inclusion can also impact the supramolecular chirality of the assemblies. Symmetry breaking is realized in an otherwise racemic coordinating assembly, and the chirality of the assembly can be facilely regulated *via* host–guest dynamics. Considering the huge potential of CD in modulating assembly pathways, CD-catalyzed assembly should receive more attention, as it has the potential to regulate the chiral or emissive properties of assemblies.

Conflicts of interest

The authors declare no conflicts of interest.

Acknowledgements

The authors are grateful to the National Natural Science Foundation of China (Grant No. 22172004, 21972003) and the Beijing National Laboratory for Molecular Sciences (BNLMS) for the financial support.

References

1 Z. Li, K. Li, M. Teng, M. Li, X. Sui, B. Liu, B. Tian and Q. Fu, *J. Mol. Liq.*, 2022, **365**, 120105.
2 K. Uekama and F. Hirayama, *Chem. Pharm. Bull.*, 1978, **26**, 1195–1200.
3 K. Uekama, A. Fujise, F. Hirayama, M. Otagiri and K. Inaba, *Chem. Pharm. Bull.*, 1984, **32**, 275–279.
4 J. Szejtli, *Starch*, 1977, **29**, 26–33.
5 V. Mohos, Z. Faisal, E. Fliszár-Nyúl, L. Szente and M. Poór, *Environ. Sci. Pollut. Res.*, 2022, **29**, 210–221.
6 Y. Liu, Y. Chen, X. Gao, J. Fu and L. Hu, *Crit. Rev. Food Sci. Nutr.*, 2022, **62**, 2627–2640.
7 A. Matencio, S. Navarro-Orcajada, F. García-Carmona and J. M. López-Nicolás, *Trends Food Sci. Technol.*, 2020, **104**, 132–143.
8 L.-Q. Peng, X. Dong, X.-T. Zhen, J. Yang, Y. Chen, S.-L. Wang, T. Xie and J. Cao, *Anal. Chim. Acta*, 2020, **1105**, 224–230.
9 A. Ghiasvand, Z. Feng and J. P. Quirino, *Anal. Chem.*, 2019, **91**, 1752–1757.
10 N. Morin-Crini, S. Fourmentin and É. Fenyvesi, *Environ. Chem. Lett.*, 2021, **19**, 2581–2617.
11 J. Szejtli, *Starch*, 1982, **34**, 379–385.
12 G. Crini, C. Bradu, M. Fourmentin, C. Cosentino, A. R. L. Ribeiro and N. Morin-Crini, *Environ. Sci. Pollut. Res.*, 2022, **29**, 171–181.
13 S. Panda and S. Fourmentin, *Environ. Sci. Pollut. Res.*, 2022, **29**, 264–270.
14 M. Yadav, S. Thakore and R. Jadeja, *Environ. Sci. Pollut. Res.*, 2022, **29**, 236–250.
15 F. Hirayama, K. Uekama and H. Koinuma, *Chem. Pharm. Bull.*, 1980, **28**, 1975–1980.
16 Z. I. Yildiz, A. Celebioglu, M. E. Kilic, E. Durgun and T. Uyar, *J. Mater. Sci.*, 2018, **53**, 15837–15849.
17 S. Deshaware, S. Gupta, R. S. Singhal, M. Joshi and P. S. Variyar, *Food Chem.*, 2018, **262**, 78–85.
18 S. A. Nepogodiev and J. F. Stoddart, *Chem. Rev.*, 1998, **98**, 1959–1976.
19 A. Harada, J. Li and M. Kamachi, *Nature*, 1992, **356**, 325–327.
20 A. Harada, J. Li and M. Kamachi, *Nature*, 1993, **364**, 516–518.
21 A. Harada, J. Li and M. Kamachi, *Nature*, 1994, **370**, 126–128.
22 R. A. Smaldone, R. S. Forgan, H. Furukawa, J. J. Gassensmith, A. M. Slawin, O. M. Yaghi and J. F. Stoddart, *Angew. Chem., Int. Ed.*, 2010, **49**, 8630–8634.
23 S. Khlifi, J. Marrot, M. Haouas, W. E. Shepard, C. Falaise and E. Cadot, *J. Am. Chem. Soc.*, 2022, **144**, 4469–4477.
24 P. Yang, W. Zhao, A. Shkurenko, Y. Belmabkhout, M. Eddaoudi, X. Dong, H. N. Alshareef and N. M. Khashab, *J. Am. Chem. Soc.*, 2019, **141**, 1847–1851.
25 L. Ni, J. Gu, X. Jiang, H. Xu, Z. Wu, Y. Wu, Y. Liu, J. Xie, Y. Wei and G. Diao, *Angew. Chem., Int. Ed.*, 2023, **62**(36), e202306528.
26 Z.-G. Jiang, W.-T. Mao, D.-P. Huang, Y. Wang, X.-J. Wang and C.-H. Zhan, *Nanoscale*, 2020, **12**, 10166–10171.
27 L. Jiang, Y. Peng, Y. Yan, M. Deng, Y. Wang and J. Huang, *Soft Matter*, 2010, **6**, 1731–1736.
28 L. Jiang, Y. Yan and J. Huang, *Soft Matter*, 2011, **7**, 10417–10423.
29 L. Jiang, Y. Yan and J. Huang, *Adv. Colloid Interface Sci.*, 2011, **169**, 13–25.
30 K. Liu, C. Ma, T. Wu, W. Qi, Y. Yan and J. Huang, *Curr. Opin. Colloid Interface Sci.*, 2020, **45**, 44–56.
31 L. Zhao, L. Jiang, Y. Han, Z. Xian, J. Huang and Y. Yan, *Soft Matter*, 2013, **9**, 7710–7717.
32 T. Gu, J. Huang and Y. Yan, *Soft Matter*, 2022, **18**, 4372–4377.
33 W. Zhi, Z. Pu, C. Ma, K. Liu, X. Wang, J. Huang, Y. Xiao and Y. Yan, *ACS Nano*, 2021, **15**, 19621–19628.
34 Z. Juvancz, R. Bodáné-Kendrovics, Z. Laczkó, R. Iványi and E. Varga, *Molecules*, 2022, **27**, 8718.
35 G. K. E. Scriba, *TrAC, Trends Anal. Chem.*, 2019, **120**, 115639.
36 Y. Wang, Y. Sun, H. Bian, L. Zhu, D. Xia and H. Wang, *ACS Appl. Mater. Interfaces*, 2020, **12**, 45916–45928.

37 L. Yue, H. Ai, Y. Yang, W. Lu and L. Wu, *Chem. Commun.*, 2013, **49**, 9770–9772.
38 J. Liang, P. Guo, X. Qin, X. Gao, K. Ma, X. Zhu, X. Jin, W. Xu, L. Jiang and P. Duan, *ACS Nano*, 2020, **14**, 3190–3198.
39 Y. Akae, H. Sogawa and T. Takata, *Bull. Chem. Soc. Jpn.*, 2019, **92**, 1413–1418.
40 L. Ji, Q. He, D. Niu, J. Tan, G. Ouyang and M. Liu, *Chem. Commun.*, 2019, **55**, 11747–11750.
41 F. Xie, G. Ouyang, L. Qin and M. Liu, *Chem. – Eur. J.*, 2016, **22**, 18208–18214.
42 Y. Zhang, D. Yang, J. Han, J. Zhou, Q. Jin, M. Liu and P. Duan, *Langmuir*, 2018, **34**, 5821–5830.
43 J. Fonseca, T. Gong, L. Jiao and H.-L. Jiang, *J. Mater. Chem. A*, 2021, **9**, 10562–10611.
44 O. M. Yaghi, G. Li and H. Li, *Nature*, 1995, **378**, 703–706.
45 S.-i Noro, R. Kitaura, M. Kondo, S. Kitagawa, T. Ishii, H. Matsuzaka and M. Yamashita, *J. Am. Chem. Soc.*, 2002, **124**, 2568–2583.
46 H. Lu, X. Yang, S. Li, Y. Zhang, J. Sha, C. Li and J. Sun, *Inorg. Chem. Commun.*, 2015, **61**, 48–52.
47 J. Liu, T.-Y. Bao, X.-Y. Yang, P.-P. Zhu, L.-H. Wu, J.-Q. Sha, L. Zhang, L.-Z. Dong, X.-L. Cao and Y.-Q. Lan, *Chem. Commun.*, 2017, **53**, 7804–7807.
48 J.-Q. Sha, X.-H. Zhong, L.-H. Wu, G.-D. Liu and N. Sheng, *RSC Adv.*, 2016, **6**, 82977–82983.
49 J. Sha, X. Yang, L. Sun, X. Zhang, S. Li, J. Li and N. Sheng, *Polyhedron*, 2017, **127**, 396–402.
50 Y. Furukawa, T. Ishiwata, K. Sugikawa, K. Kokado and K. Sada, *Angew. Chem., Int. Ed.*, 2012, **51**, 10566–10569.
51 B. Liu, Y. He, L. Han, V. Singh, X. Xu, T. Guo, F. Meng, X. Xu, P. York, Z. Liu and J. Zhang, *Cryst. Growth Des.*, 2017, **17**, 1654–1660.
52 Y. Wei, D. Sun, D. Yuan, Y. Liu, Y. Zhao, X. Li, S. Wang, J. Dou, X. Wang, A. Hao and D. Sun, *Chem. Sci.*, 2012, **3**, 2282–2287.
53 L. Han, T. Guo, Z. Guo, C. Wang, W. Zhang, S. Shakya, H. Ding, H. Li, X. Xu, Y. Ren and J. Zhang, *J. Phys. Chem. B*, 2018, **122**, 5225–5233.
54 M. Shen, J. Zhou, M. Elhadidy, Y. Xianyu, J. Feng, D. Liu and T. Ding, *Ultrason. Sonochem.*, 2022, **86**, 106003.
55 M. S. Samuel, J. Bhattacharya, C. Parthiban, G. Viswanathan and N. D. Pradeep Singh, *Ultrason. Sonochem.*, 2018, **49**, 215–221.
56 J. J. Gassensmith, R. A. Smaldone, R. S. Forgan, C. E. Wilmer, D. B. Cordes, Y. Y. Botros, A. M. Z. Slawin, R. Q. Snurr and J. F. Stoddart, *Org. Lett.*, 2012, **14**, 1460–1463.
57 H. Li, N. Lv, X. Li, B. Liu, J. Feng, X. Ren, T. Guo, D. Chen, J. Fraser Stoddart, R. Gref and J. Zhang, *Nanoscale*, 2017, **9**, 7454–7463.
58 K. J. Hartlieb, D. P. Ferris, J. M. Holcroft, I. Kandela, C. L. Stern, M. S. Nassar, Y. Y. Botros and J. F. Stoddart, *Mol. Pharmaceutics*, 2017, **14**, 1831–1839.
59 S. Han, Y. Wei, C. Valente, R. S. Forgan, J. J. Gassensmith, R. A. Smaldone, H. Nakanishi, A. Coskun, J. F. Stoddart and B. A. Grzybowski, *Angew. Chem., Int. Ed.*, 2011, **50**, 276–279.
60 Z.-J. Qiu, S.-T. Fan, C.-Y. Xing, M.-M. Song, Z.-J. Nie, L. Xu, S.-X. Zhang, L. Wang, S. Zhang and B.-J. Li, *ACS Appl. Mater. Interfaces*, 2020, **12**, 55299–55307.
61 K. J. Hartlieb, J. M. Holcroft, P. Z. Moghadam, N. A. Vermeulen, M. M. Algaradah, M. S. Nassar, Y. Y. Botros, R. Q. Snurr and J. F. Stoddart, *J. Am. Chem. Soc.*, 2016, **138**, 2292–2301.
62 L. Li, J. Wang, Z. Zhang, Q. Yang, Y. Yang, B. Su, Z. Bao and Q. Ren, *ACS Appl. Mater. Interfaces*, 2019, **11**, 2543–2550.
63 X. Dai, L. Tian, Z. Liu, W. Xu, Y.-P. Liu and Y. Liu, *ACS Nano*, 2022, **16**, 18398–18407.
64 W. Xu, L.-H. Wang, Y. Chen and Y. Liu, *Mater. Today Chem.*, 2022, **24**, 100896.
65 Y. Chen, B. Yu, Y. Cui, S. Xu and J. Gong, *Chem. Mater.*, 2019, **31**, 1289–1295.
66 L. Hu, K. Li, W. Shang, X. Zhu and M. Liu, *Angew. Chem., Int. Ed.*, 2020, **59**, 4953–4958.
67 M. Peng, A. M. Kaczmarek and K. Van Hecke, *ACS Appl. Mater. Interfaces*, 2022, **14**, 14367–14379.
68 X.-Y. Chen, H. Chen, L. Đorđević, Q.-H. Guo, H. Wu, Y. Wang, L. Zhang, Y. Jiao, K. Cai, H. Chen, C. L. Stern, S. I. Stupp, R. Q. Snurr, D. Shen and J. F. Stoddart, *J. Am. Chem. Soc.*, 2021, **143**, 9129–9139.
69 D. Shen, G. Wang, Z. Liu, P. Li, K. Cai, C. Cheng, Y. Shi, J.-M. Han, C.-W. Kung, X. Gong, Q.-H. Guo, H. Chen, A. C. H. Sue, Y. Y. Botros, A. Facchetti, O. K. Farha, T. J. Marks and J. F. Stoddart, *J. Am. Chem. Soc.*, 2018, **140**, 11402–11407.
70 L. Xu, C.-Y. Xing, D. Ke, L. Chen, Z.-J. Qiu, S.-L. Zeng, B.-J. Li and S. Zhang, *ACS Appl. Mater. Interfaces*, 2020, **12**, 3032–3041.
71 V. Singh, T. Guo, H. Xu, L. Wu, J. Gu, C. Wu, R. Gref and J. Zhang, *Chem. Commun.*, 2017, **53**, 9246–9249.
72 V. Singh, T. Guo, L. Wu, J. Xu, B. Liu, R. Gref and J. Zhang, *RSC Adv.*, 2017, **7**, 20789–20794.
73 H. Li, M. R. Hill, R. Huang, C. Doblin, S. Lim, A. J. Hill, R. Babarao and P. Falcaro, *Chem. Commun.*, 2016, **52**, 5973–5976.
74 D. Ke, J.-F. Feng, D. Wu, J.-B. Hou, X.-Q. Zhang, B.-J. Li and S. Zhang, *RSC Adv.*, 2019, **9**, 18271–18276.
75 M. R. Horn, A. Singh, S. Alomari, S. Goberna-Ferrón, R. Benages-Vilau, N. Chodankar, N. Motta, K. Ostrikov, J. MacLeod, P. Sonar, P. Gomez-Romero and D. Dubal, *Energy Environ. Sci.*, 2021, **14**, 1652–1700.
76 J.-X. Liu, X.-B. Zhang, Y.-L. Li, S.-L. Huang and G.-Y. Yang, *Coord. Chem. Rev.*, 2020, **414**, 213260.
77 M. Stuckart and K. Y. Monakhov, *Chem. Sci.*, 2019, **10**, 4364–4376.
78 M. Noltemeyer and W. Saenger, *Nature*, 1976, **259**, 629–632.
79 Y. Wu, R. Shi, Y.-L. Wu, J. M. Holcroft, Z. Liu, M. Frasconi, M. R. Wasielewski, H. Li and J. F. Stoddart, *J. Am. Chem. Soc.*, 2015, **137**, 4111–4118.
80 B. Zhang, W. Guan, F. Yin, J. Wang, B. Li and L. Wu, *Dalton Trans.*, 2018, **47**, 1388–1392.
81 C. Falaise, M. A. Moussawi, S. Floquet, P. A. Abramov, M. N. Sokolov, M. Haouas and E. Cadot, *J. Am. Chem. Soc.*, 2018, **140**, 11198–11201.
82 J. Joseph, C. A. Dreiss, T. Cosgrove and J. S. Pedersen, *Langmuir*, 2007, **23**, 460–466.
83 J. Puig-Rigall, I. Grillo, C. A. Dreiss and G. González-Gaitano, *Langmuir*, 2017, **33**, 4737–4747.
84 S. Sen, B. K. Paul and N. Guchhait, *J. Mol. Liq.*, 2019, **274**, 584–591.
85 H. Xu and Y. Yao, *Supramol. Chem.*, 2017, **29**, 161–166.
86 A. González-Pérez, J. Carlstedt, R. S. Dias and B. Lindman, *Colloids Surf., B*, 2010, **76**, 20–27.
87 S. Kumari, S. Halder, R. Aggrawal, V. K. Aswal, G. Sundar and S. K. Saha, *J. Mol. Liq.*, 2020, **300**, 112238.
88 A. Harada, J. Li and M. Kamachi, *Macromolecules*, 1993, **26**, 5698–5703.
89 J. Li, A. Harada and M. Kamachi, *Polym. J.*, 1994, **26**, 1019–1026.
90 A. Domiński, T. Konieczny and P. Kurcok, *Materials*, 2020, **13**, 133.
91 L. Jiang, Y. Peng, Y. Yan and J. Huang, *Soft Matter*, 2011, **7**, 1726–1731.
92 C. Zhou, X. Cheng, Q. Zhao, Y. Yan, J. Wang and J. Huang, *Langmuir*, 2013, **29**, 13175–13182.
93 C. Zhou, X. Cheng, Y. Yan, J. Wang and J. Huang, *Langmuir*, 2014, **30**, 3381–3386.
94 S. Yang, Y. Yan, J. Huang, A. V. Petukhov, L. M. J. Kroon-Batenburg, M. Drechsler, C. Zhou, M. Tu, S. Granick and L. Jiang, *Nat. Commun.*, 2017, **8**, 15856.
95 C. Zhou, J. Huang and Y. Yan, *Soft Matter*, 2016, **12**, 1579–1585.
96 C. Zhou, X. Cheng, Q. Zhao, Y. Yan, J. Wang and J. Huang, *Sci. Rep.*, 2014, **4**, 7533.
97 W. Qi, X. Wang, Z. Liu, K. Liu, Y. Long, W. Zhi, C. Ma, Y. Yan and J. Huang, *J. Colloid Interface Sci.*, 2021, **597**, 325–333.
98 X. Wang, M. Li, P. Song, X. Lv, Z. Liu, J. Huang and Y. Yan, *Chem. – Eur. J.*, 2018, **24**, 13734–13739.
99 L. Jiang, J. W. de Folter, J. Huang, A. P. Philipse, W. K. Kegel and A. V. Petukhov, *Angew. Chem., Int. Ed.*, 2013, **52**, 3364–3368.
100 K. Harata, *Bioorg. Chem.*, 1981, **10**, 255–265.
101 H. Kazuaki and U. Hisashi, *Bull. Chem. Soc. Jpn.*, 1975, **48**, 375–378.
102 K. Masato and F. Toshio, *Bull. Chem. Soc. Jpn.*, 1986, **59**, 2032–2034.
103 R. Krishnan, A. M. Rakhi and K. R. Gopidas, *J. Phys. Chem. C*, 2012, **116**, 25004–25014.
104 W. Qi, C. Ma, Y. Yan and J. Huang, *Curr. Opin. Colloid Interface Sci.*, 2021, **56**, 101526.
105 X. Wang, W. Zhi, C. Ma, Z. Zhu, W. Qi, J. Huang and Y. Yan, *JACS Au*, 2021, **1**, 156–163.

106 X. L. Ni, S. Chen, Y. Yang and Z. Tao, *J. Am. Chem. Soc.*, 2016, **138**, 6177–6183.
107 X. Shi, J. Zhang, J. Liu, X. Zhao, H. Wang, P. Wei, X. Zhang, X.-L. Ni, H. H.-Y. Sung, I. D. Williams, W. K. Ng, K. S. Wong, J. W. Y. Lam, L. Wang, H. Jin and B. Z. Tang, *Angew. Chem., Int. Ed.*, 2022, **61**, e202211298.
108 J. Wang, Z. Huang, X. Ma and H. Tian, *Angew. Chem., Int. Ed.*, 2020, **59**, 9928–9933.
109 Z.-Y. Zhang, W.-W. Xu, W.-S. Xu, J. Niu, X.-H. Sun and Y. Liu, *Angew. Chem., Int. Ed.*, 2020, **59**, 18748–18754.
110 K. N. Houk, A. G. Leach, S. P. Kim and X. Zhang, *Angew. Chem., Int. Ed.*, 2003, **42**, 4872–4897.